Entanglement Effects in Polyethylene Melts: ^{13}C NMR Relaxation Experiments†

XiaoHua Qiu and M. D. Ediger*

Department of Chemistry, University of Wisconsin−Madison, Madison, Wisconsin 53706

Received April 5, 2001

ABSTRACT: ^{13}C NMR T_1, NOE, and $T_{1\rho}$ were measured for two entangled polyethylene melts ($M = 16K$ and 37K) at 5 and 75 MHz ^{13}C Larmor frequencies from the melting point up to 530 K. Two models for entanglement dynamics are tested against the experimental data. This comparison shows that entanglements not only stretch out those relaxation times longer than the entanglement time τ_e but also have a spatial effect in restricting the motion of entangled points on the time scale of τ_e. For polyethylene, the amplitude of residual orientation on the time scale of τ_e is lower than the theoretical prediction for a Gaussian chain of the entanglement length with both ends fixed. The opposite conclusion was drawn from recent double quantum NMR experiments on polybutadiene. The magnetization decay curve for the $T_{1\rho}$ experiment is nonexponential, indicating that the loss of orientation on long time scales depends on position along the chain backbone.

I. Introduction

Polymer dynamics occur over a wide range of time scales from nanoseconds (segmental relaxation far above T_g) to seconds and beyond (terminal relaxation at lower temperatures). Global dynamics largely determine the practical viscoelastic behavior of polymer melts. Segmental dynamics are the fundamental motions that drive all the slower time scale global dynamics. Segmental dynamics also directly determine the glass transition temperature T_g and small molecule transport properties in the polymer matrix.

Powerful NMR techniques have been invented to probe polymer dynamics for the whole range of relaxation processes. NMR methods provide several advantages over other experimental methods. First, a variety of nuclei can be utilized; ^1H, ^{13}C, ^{31}P, and ^{19}F are often found in polymer systems. Second, sensitivity toward different chemical structures allows the investigation of dynamics for chemically distinctive sites in homopolymers or individual components in a complex system such as a polymer blend. Third, single particle correlation functions can be measured in some circumstances and are easier to interpret than observables sensitive to collective motions.

Traditionally, different NMR methods have been used to probe segmental dynamics and global dynamics. NMR spin−lattice relaxation measurements, namely the spin−lattice relaxation time T_1 and the nuclear Overhauser effect (NOE), are reliable methods to characterize segmental dynamics. ^2H and ^{13}C NMR are used most often because their signals can be described entirely by a single particle correlation function and thus are the easiest to analyze. Experiments and MD simulations show that segmental dynamics can be successfully described by a stretched exponential function.[1−3]

Spin−spin relaxation measurements and several modern modifications have been introduced to measure the global dynamics of polymer melts and networks.[4−9] Since the signal is weak in this case, most experiments work with ^1H NMR. These methods are based on monitoring the weak (residual) proton dipolar interactions, as suggested by Cohen-Addad[10] shortly after the introduction of the reptation model.[11] In general, ^1H magnetization decays are difficult to interpret since many ^1H pairs contribute to the signal, including pairs on different chains. However, in the case of global dynamics, it is accepted that signals associated with interchain ^1H pairs decay away quickly, and the long time correlation function can be treated as a single particle correlation function.[4]

These two different NMR methods are conceptually linked since they both probe the reorientation dynamics of vectors between two neighboring nuclei on a chain. The weak (residual) dipolar interactions used to study global dynamics by NMR are the result of incomplete randomization by the segmental dynamics that can be characterized by T_1 and NOE experiments. Yet connections between the two NMR approaches have been fairly primitive. In the case of T_1 and NOE measurements, the global dynamics are often ignored[12] or treated as a generic tail function.[13] On the other hand, the effect of segmental dynamics is often only an adjustable parameter[14] for experiments studying global dynamics.

The reason for this lack of connection between the two approaches resides in the very different time scales probed by each method. Conventional T_1 and NOE experiments typically are most sensitive to dynamics occurring from several hundred picoseconds to several nanoseconds. The time scale probed by the second approach ranges from several microseconds to tens of milliseconds. Thus, the lack of effective experimental methods to probe the dynamics in the range of 10^{-6}−10^{-9} s made a quantitative connection between the two approaches difficult.

In this study, we make a quantitative connection between segmental and global dynamics for entangled polyethylene (PE). ^{13}C T_1 and NOE experiments were performed on this system from 400 to 530 K at 5 and 75 MHz ^{13}C Larmor frequency. Several factors are crucial for this progress. The unusually low Larmor frequency of 5 MHz extends the effective time scale

† This paper is dedicated to Prof. Hans Sillescu on his 65th birthday.

* To whom correspondence should be addressed.

10.1021/ma010597i CCC: $22.00
Published on Web 01/26/2002

probed by T_1 and NOE measurements to more than 30 ns so we reduce the experimentally inaccessible time window by an order of magnitude. The segmental dynamics of PE melts are unusually fast which focuses the experimental frequency range on the transition from segmental dynamics to global dynamics. In addition, a wide temperature range provides an effective way to shift the time scale of polymer dynamics. Knowledge gained in our previous study of the segmental and global dynamics of unentangled PE melts[15] provides us with a solid starting point for the analysis of entangled melts in this study. In particular, that work showed that C−H vector reorientation in PE has an unusually large contribution from global dynamics[16] which helps to alleviate the inefficiency of probing global dynamics using spin−lattice relaxation experiments.

Two models for entanglement dynamics are tested against the experimental data. This comparison shows that entanglements not only stretch out those relaxation times longer than the entanglement time τ_e but also have a spatial effect in restricting the motion of entangled points on the time scale of τ_e. For PE, the amplitude of residual orientation on the time scale of τ_e is lower than the theoretical prediction for a Gaussian chain of the entanglement length with both ends fixed.

We also explore the possibility of probing the global dynamics of entangled PE using $T_{1\rho}$ experiments. The $T_{1\rho}$ magnetization decay curve for a sample with M = 16K is nonexponential while our earlier studies found that the same kind of curve is exponential for unentangled PE (M = 2K). The nonexponential decay indicates that the loss of orientation on long time scales depends on position along the chain backbone.

II. Experimental Section

Materials. Hydrogenated polybutadiene, denoted as PE16K (M_w = 15 700, M_w/M_n = 1.08, 2% ethyl branches), was purchased from Scientific Polymer. Low-density PE, denoted as PE37K (M_w = 37K, M_w/M_n = 3.6, <1% branches), was provided by ExxonMobil Co.

NMR Measurements. Both samples contained 1 g of material in a 10 mm Wilmad NMR sample tube. The samples were degassed under vacuum for 1 day at room temperature, then for another day above the melting temperature, and finally sealed under vacuum. Methylene units on the backbone of PE show up as a dominating peak in the ^{13}C NMR spectrum at 30 ppm. All measurements were performed at 75.47 or 5.06 MHz ^{13}C Larmor frequencies on a Bruker DMX-300 spectrometer specially designed for frequent field change. A homemade probe utilizing the solenoid geometry and optimized for high-temperature experiments was used.[18] Temperature was calibrated by observing the sudden spectrum change as the melting point of chosen compounds (T_m from 333 to 533 K) was crossed. This calibration method yielded a temperature accuracy of ±1 K. The temperature controller was able to maintain the temperature to ±0.1 K during an experiment.

T_1 was measured by a $\pi-\tau-\pi/2$ pulse sequence, waiting at least $8T_1$ between the acquisition and the next π pulse. NOE was measured by the comparison of spectra with continuous decoupling and inverse-gated decoupling, waiting at least $10T_1$ between acquisitions. Details of the measurements have been described previously.[18] Eight and 2000 scans were collected for signal averaging for 75 and 5 MHz, respectively. T_1 values are believed to be accurate within 2%; NOEs are accurate within 0.03 for 75 MHz and 0.1 for 5 MHz.

$T_{1\rho}$ was measured by a $\pi/2-\tau$(locking) pulse sequence. Since the delay time τ might be long for the experiment, only very weak locking power was employed to avoid heating the sample. The actual power used was equivalent to the magnetic field for 2 kHz ^{13}C Larmor frequency. To avoid complications from the decoupling source during the locking time, the proton decoupler was turned on only during FID collection time.[19] The center of the spectrum was carefully set to be less than 5 Hz away from the main peak to avoid any error caused by off-resonance conditions. All $T_{1\rho}$ data were collected at 75 MHz ^{13}C Larmor frequency. The resulting magnetization decay curve is not a single exponential (see Figure 6). Thus, a multiexponential function[21] was used to fit the decay curve, and the inverse averaged rate $\langle 1/T_{1\rho}\rangle^{-1}$ is reported.

Relaxation Equations. For aliphatic carbons on polymers, the only important mechanism for ^{13}C magnetization relaxation is dipolar coupling to the directly bonded protons.[15] For an isotropic system, the connection between NMR relaxation and molecular motion is made through the C−H bond vector second-order orientation autocorrelation function (OACF):[21]

$$G(t) = \frac{1}{2}\langle 3\cos^2\theta(t) - 1\rangle \tag{1}$$

where $\theta(t)$ describes the orientation of a C−H bond vector at time t relative to its orientation at time 0. The brackets indicate an average over equivalent C−H bond vectors and over all possible arbitrary starting times t = 0.

$J(\omega)$ is the Fourier transform of $G(t)$:

$$J(\omega) = \frac{1}{2}\int_{-\infty}^{+\infty} G(t)e^{i\omega t}\,dt \tag{2}$$

T_1, NOE, and $T_{1\rho}$ can be expressed in terms of $J(\omega)$:[23]

$$\frac{1}{T_1} = Kn[J(\omega_H - \omega_C) + 3J(\omega_C) + 6J(\omega_H + \omega_C)] \tag{3}$$

$$\mathrm{NOE} = 1 + \frac{\gamma_H}{\gamma_C}\left[\frac{6J(\omega_H + \omega_C) - J(\omega_H - \omega_C)}{J(\omega_H - \omega_C) + 3J(\omega_C) + 6J(\omega_H + \omega_C)}\right] \tag{4}$$

$$\frac{1}{T_{1\rho}} = \frac{1}{2}Kn[4J(\omega_e) + J(\omega_H - \omega_C) + 3J(\omega_C) + 6J(\omega_H) + 6J(\omega_H + \omega_C)] \tag{5}$$

where ω_H and ω_C are the resonance frequencies of ^{1}H and ^{13}C, ω_e is the spin-locking field, n is the number of bonded protons, K is a constant whose value is calculated to be 2.29×10^9 s^{-2},[13] and γ_H and γ_C are the gyromagnetic ratios for ^{1}H and ^{13}C.

III. Results

Figure 1 shows T_1 and NOE data of the two PE samples as a function of temperature at 5 and 75 MHz ^{13}C Larmor frequency. For the lower molecular weight sample, Figure 2 shows the reciprocal of the averaged rate for $T_{1\rho}$ as a function of temperature at 75 MHz ^{13}C Larmor frequency main field and 2 kHz locking field. The lines in this figure are predictions for PE with different molecular weights from a model described below.

IV. Discussion

A. How Does a C−H Vector Lose Its Orientation?

Since all the experimental data are determined by the reorientation of a C−H vector, an understanding of how this reorientation takes place is an essential starting point. In our previous work on linear unentangled PE melts, we showed that the distribution of relaxation times relevant for C−H vector reorientation can be broken down into two contributions.[15] Figure 3 illustrates this schematically, using a bead−spring representation. At short times (top right in Figure 3), many conformational transitions take place and almost completely relax the C−H vector orientation. However, on that short time scale, the vector does not uniformly

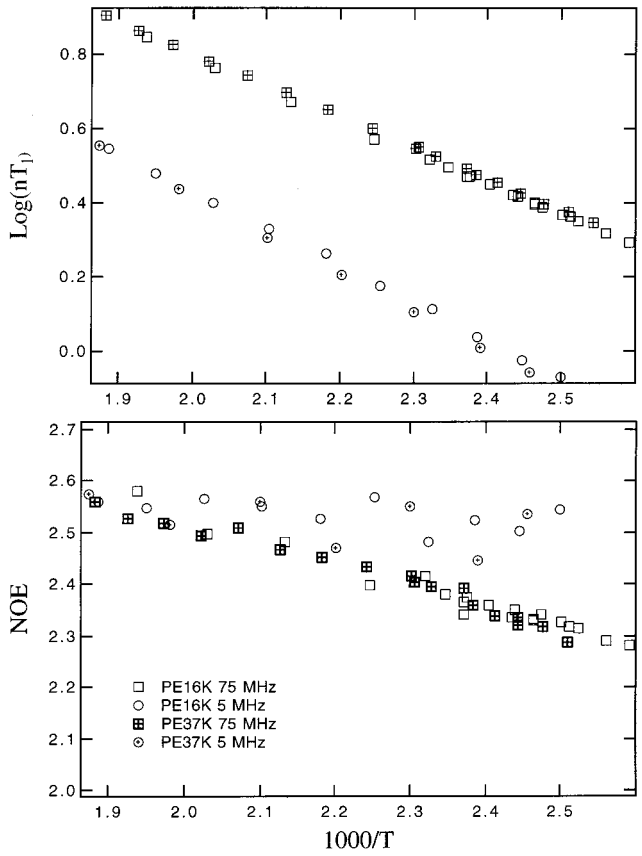

Figure 1. T_1 and NOE measurements of PE16K and PE37K at 75 and 5 MHz ^{13}C Larmor frequency. The experimental data are essentially the same for the two polyethylene melts with different molecular weight (M = 16K and 37K, respectively).

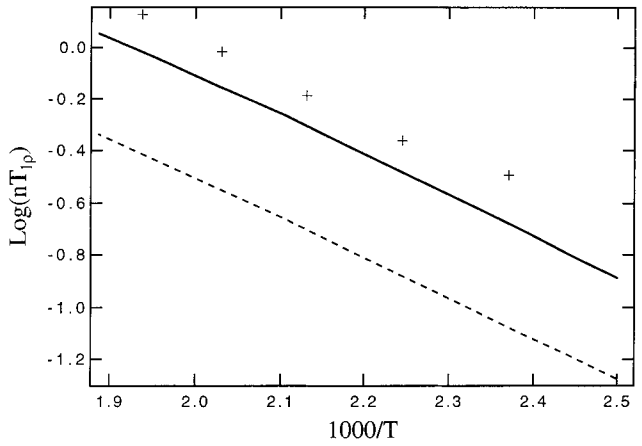

Figure 2. $T_{1\rho}$ measurements (symbols) of PE16K at 75 MHz ^{13}C Larmor frequency main field and 2 kHz locking field. Since the magnetization decay curve is not exponential, the reciprocal of the averaged rate is plotted. The solid line is the prediction for PE16K from model II (described in the text). The dashed line is the prediction using the same model for PE31K. The differences between the two predictions indicate $T_{1\rho}$ is likely to be very sensitive to molecular weight difference in this region.

explore all orientations but rather has some tendency to be perpendicular to a vector which describes the local chain orientation. This local orientation or "spring" vector is shown in Figure 3 as connecting two adjacent beads. At long times (bottom right in Figure 3), the spring vector reorients significantly, and C−H vector randomization is complete. (The center right portion of Figure 3 is discussed below.)

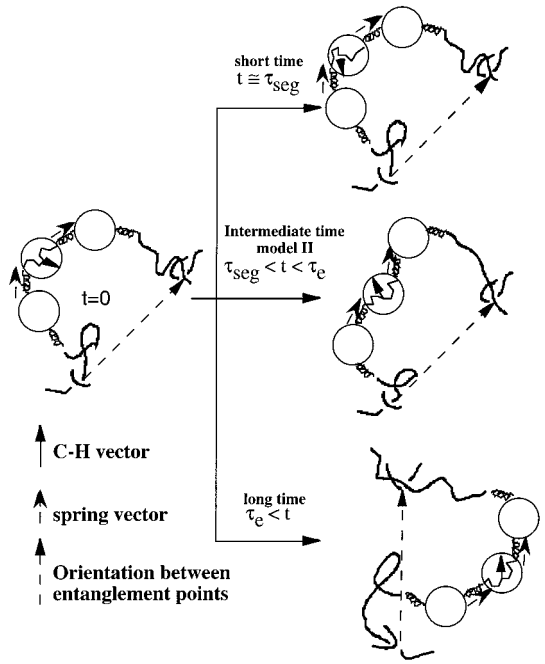

Figure 3. Mapping of C−H vector reorientation in polyethylene onto the bead−spring model with entanglement effects. At times comparable to the segmental relaxation time τ_{seg}, conformational transitions take place and partially relax the C−H vector orientation. However, on that short time scale, the vector connecting two beads (the spring vector) cannot reorient significantly, so the C−H vector does not uniformly explore all possible orientations but rather has some tendency to be perpendicular to the spring vector. At times longer than τ_{seg} but shorter than the entanglement time τ_e, the spring vector partially loses its initial orientation, but the vector connecting two entanglement points cannot reorient significantly. There is residual orientation left on that time scale. This representation assumes that entanglements have a spatial effect in restricting motions of the end points of entanglements (model II). Only at times longer than the disentanglement time of the chain is C−H vector randomization complete.

Mathematically, these two contributions to the orientation autocorrelation function (OACF) can be written as

$$G(t) = A_{seg}G_{seg}(t) + (1 - A_{seg})G_{nm}(t) \qquad (6)$$

where A_{seg} is the fraction of the correlation function decay due to segmental dynamics. A_{seg} is determined by the residual orientation of a C−H vector after many conformational transitions have occurred but before the reorientation of a section of the chain represented by the spring vector in Figure 3. A_{seg} is independent of molecular weight for chains longer than several statistical segments. $G_{seg}(t)$ is a function describing the decay of the OACF caused by segmental dynamics; this component is essentially independent of molecular weight. $G_{nm}(t)$ is a function describing the decay of the OACF caused by normal mode relaxation; this component depends on the length and architecture of the chain.

While there is little controversy on how to model $G_{nm}(t)$ for an unentangled chain (details are described in ref 15), modeling entanglement effects in $G_{nm}(t)$ is rather controversial. Two models were tested to describe the experimental data for PE16K.

Model I treats the entanglement as only having a time effect and is consistent with the treatment proposed by

Brereton.[23] C−H vector reorientation evolves from the top right frame of Figure 3 at short time to bottom right frame for long time without a distinctive intermediate stage. $G_{nm}(t)$ is treated as a Rouse[24] chain with corrections for entanglements[25] in that relaxation times for Rouse segments longer than the entanglement length M_e are scaled by $(M/M_e)^{3.4}$. M_e is treated as a fitting parameter in our implementation of this model. The procedure used to calculate the C−H vector OACF from the normal modes is described in a previous paper.[16]

Model II, sometimes called the hierarchy model, adds a spatial component for the entanglement effects. It is consistent with the treatment proposed by Cohen-Addad[14] and further developed by Kimmich[26] and Callaghan and Samulski.[27] In this model, normal mode motions are divided into three characteristic time regimes. For times less than τ_e, the Rouse time for a chain of entanglement molecular weight, the normal modes relax according to Rouse dynamics with the special condition that motion is restricted at entanglement points (illustrated in the center right frame in Figure 3). These dynamics relax most of the orientation left after segmental dynamics. Because of the restricted entanglement points, a very small residual orientation A_{ent} is still left to be further relaxed by slower motions. This small residual orientation is shown in Figure 3 as a long arrow with a dashed line. For times in between τ_e and the Rouse time τ_R, the normal modes relax according to Rouse motion constrained to a tube. For times longer than τ_R, the motion becomes curvilinear diffusion in the tube. No orientation remains beyond the tube disentanglement time, τ_d. Because of our frequency range, we are only sensitive to the first two regions. M_e and A_{ent} are treated as fitting parameters in our implementation of the model. Detailed procedures for this implementation are described in the Appendix.

B. Testing of the Models. The best fits from the two models are plotted in Figure 4. The parameters used are summarized in Table 1 with the free fitting parameter values in italics. An explanation of the parameter values is given in the next paragraph. The most important feature in these comparisons is that the fits from model II give a qualitatively better description of the data than model I. This comparison strongly suggests that entanglements have both temporal and spatial effects on the reorientation of C−H vectors.

All the fixed parameter values in our fitting procedure come from our study of unentangled PE and other independent experiments. From our previous work, we get the values for τ_{seg}, $E_{a,seg}$, A_{seg}, and τ_{44}/τ_{seg}. τ_{44} is the relaxation time for a Rouse segment with 44 carbons. $E_{a,seg}$ is the activation energy for segmental dynamics. $E_{a,seg}$ and A_{seg} do not depend on molecular weight when the chain is at least a few repeat units long. The ratio τ_{44}/τ_{seg} is also molecular weight independent once the chain is more than 44 carbons long. For these three parameters, values from our previous work are directly employed. A direct application of $\tau_{seg} = 5$ ps at 400 K as found in our previous work does not yield satisfactory agreement with the experimental data for either model. Although τ_{seg} is almost independent of molecular weight, it is likely to be influenced by the change in monomer friction coefficient ζ. Since ζ for PE16K is 1.5 times larger than that for $M = 2150$ g/mol,[29] 7.5 ps is used as τ_{seg} at 400 K for our analysis. The value for the activation energy of global motions is set equal to the flow activation energy of 6.4 kcal/mol.[25]

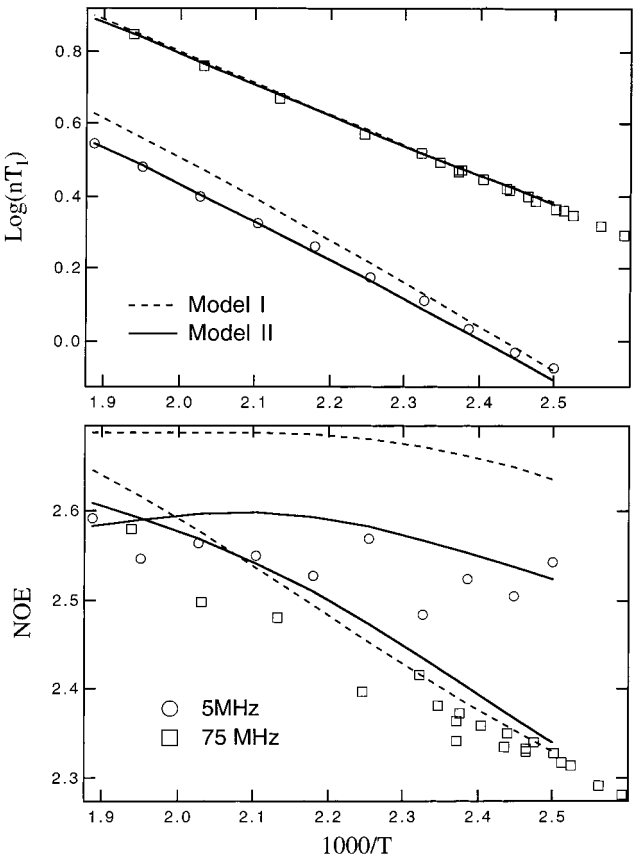

Figure 4. Fits of T_1 and NOE data to models for polymer melt dynamics described in the text. The dashed lines are for model I, and the solid lines are for model II. Model II provides qualitatively better predictions than model I. Since the only difference in the two models are how entanglement effects are included, this figure shows the sensitivity of our data toward the entanglement effect. Model II, which treats entanglements as having both temporal and spatial effect, is a better description of the system than model I, which treats entanglements as only having a temporal effect.

Table 1. Parameters Used for Models I and II

	model I	model II
τ_{seg}(400 K)	7.5 ps	7.5 ps
A_{seg}	$A_{seg}(T)^a$	$A_{seg}(T)^a$
$E_{a,seg}$	4.0 kcal/mol	4.0 kcal/mol
τ_{44} (400 K)	4.5 ns	4.5 ns
$E_{a,nm}$	6.4 kcal/mol	6.4 kcal/mol
M_e	*1000 g/mol*	*1000 g/mol*
A_{ent}	NA	*0.02*

[a] $A_{seg}(T) = 0.915 + 73.957/T - 22688/T^2$.

It might be argued that model II fits better than model I because it has an additional fitting parameter. We systematically adjusted all the parameters in model I, yet no adjustment could make its predictions similar in quality to model II. In addition, fixing the fitting parameters in model II over a range of reasonable values results in better agreement with the experimental data than for model I. Thus, the discrimination between the models indicates model II is fundamentally superior. We interpret this to mean that the spatial restrictions caused by entanglements on the time scale of τ_e cannot be ignored in modeling the reorientation of a C−H vector. In earlier work on atactic polypropylene (aPP), we showed that model I did provide a satisfactory fit.[16] Since the amplitude of global motions for that system is more than a factor of 10 smaller than PE, that

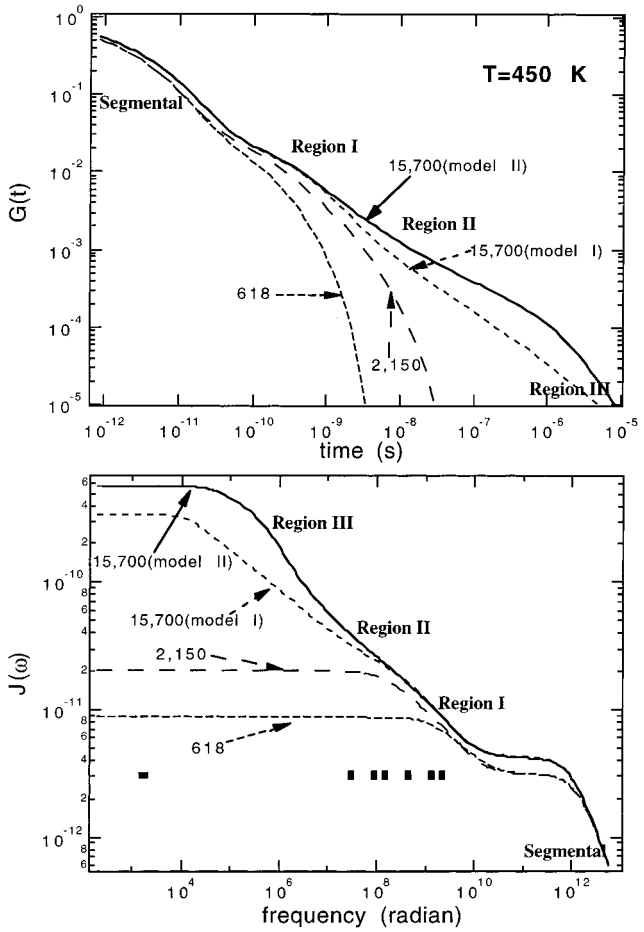

Figure 5. Orientation autocorrelation function $G(t)$ and its Fourier transform $J(w)$ at 450 K generated by the best fits to data for three polyethylene samples ($M = 618$, $M = 2150$, and $M = 15\,700$ g/mol). For the highest molecular weight sample, best fits from two models are plotted. The functions can be broken into two parts: segmental and global dynamics (subdivided into regions I, II, and III). For model II, region I corresponds to free Rouse motion between entanglements, region II corresponds to Rouse motion restricted to a tube, and region III corresponds to curvilinear diffusion along the tube. For model I, region I corresponds to normal model motions for Rouse segments less than the entanglement length. In regions II and III, relaxation times are stretched due to entanglements but no spatial constraints are incorporated. In the lower panel, the frequencies probed by T_1 and NOE measurements are plotted as solid vertical bars, and the additional frequency probed by $T_{1\rho}$ experiments is plotted as a horizontal bar. The overlap of the former frequencies with regions I and II explains why the experiment is sensitive to the entanglement effects.

fit was not very sensitive to the exact shape of the OACF of global motions. After publication of ref 16, we also applied model II to our aPP data, and the fits are equally satisfactory.

Figure 5 shows the OACF $G(t)$ and its Fourier transform $J(w)$ for the two models (curves labeled "15,700"). Also shown are previously obtained curves for two lower molecular weight PE samples. The regions corresponding to segmental dynamics are indicated. For the high molecular weight samples, longer time and length scale motions are divided into three regions. Region I corresponds to Rouse motion between entanglements, region II corresponds to the Rouse motion restricted to a tube, and region III corresponds to curvilinear diffusion in a tube. (Model I does not distinguish between regions II and III.)

It is clear from Figure 5 that the two models for the dynamics of PE16K differ only in the time region close to and beyond τ_e (transition from region I to II). The experimentally probed frequency range is shown in the $J(\omega)$ plot. It is the overlap of this frequency range with region I and II that makes the current experiment an effective way to probe the effects of the onset of entanglement. We plot region III in the figure only because it illustrates model II clearly. We do not claim to test this part quantitatively since we only have very limited sensitivity in this region through $T_{1\rho}$ experiments. Transverse relaxation measurements employing residual proton dipolar interactions are more appropriate for studying dynamics in region III.

C. Entanglement Molecular Weight and Effects of Entanglement. The M_e which results from fitting model II (1000 g/mol) agrees nicely with the value of 830 g/mol calculated from plateau modulus G_N^0.[30] Neutron spin-echo experiments (NSE) also provide microscopic measurement for this important parameter. However, the M_e measured by NSE[30] (2000 g/mol) is more than twice that calculated from G_N^0. The agreement is even poorer if one considers recent MD simulations by Pütz et al.[31] suggesting that the actual M_e determined from NSE should be 2.3 times less than the M_e determined from G_N^0. Direct comparison of that simulation with our NMR experiment is difficult since $G(t)$ has not been reported. In contrast to the results reported here, previous NMR determinations of M_e[32] have yielded values considerably larger than that determined from plateau modulus.

The second parameter that also strongly influences the shape of OACF is the residual orientation on the time scale of τ_e. Cohen-Addad has estimated this by modeling an entanglement as a Gaussian chain with both ends fixed.[10] If the chain has N_k Kuhn segments (corresponding to M_e), the residual orientation is $3/(5N_k)$. N_k for M_e of 1000 g/mol is around 7, giving a residual amplitude of 10%. Fits to the experimental data result in a significantly smaller number (2%), suggesting that the end points of the entangled segment are not completely frozen on the time scale of τ_e. This is consistent with the picture that entanglement is a dynamical process, and entanglement points also evolve on the time scale of τ_e.

D. Connection to Other Experimental Methods. As mentioned in the Introduction, several groups have employed variations of NMR transverse relaxation measurements to probe the slow dynamics of polymer melts. All of these measurements start with a preaveraged magnetization since segmental motions are much faster than the times probed by these experiments. The amplitude of this preaveraged magnetization cannot be directly observed except in the case of a recent ^{1}H double quantum experiment.[6]

Our work shows that the so-called preaveraged magnetization can be broken into two parts. The first averaging caused by segmental dynamics leaves a residual orientation of about 0.1−5% in the OACF. This amplitude is determined by the stiffness of the repeat units and the local orientation freedom.[33] Our studies of PE and aPP show that this amplitude can vary by an order of magnitude for different polymers.[15,16] The second part of this preaveraging is associated with Rouse dynamics of the Kuhn segments in between entanglement points where the entanglement points are restricted in space. The 2% residual orientation ex-

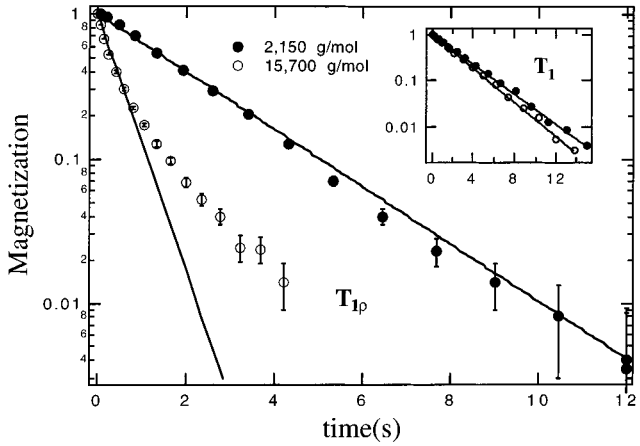

Figure 6. Magnetization decay for $T_{1\rho}$ experiments on PE melts of two different molecular weights. The inset compares the magnetization decay for T_1 experiments at the same temperature. The $T_{1\rho}$ decay for the high molecular weight PE is clearly nonexponential. These results indicate that the fast segmental dynamics probed by T_1 are homogeneous over all chain positions while the slow global dynamics, to which $T_{1\rho}$ is also sensitive, depend on position along the chain backbone.

tracted from these measurements (see above) characterizes only this second part.

In their recent work on polybutadiene, Graf et al.[6] found a residual orientation at τ_e much larger than that predicted for a Gaussian chain of one entanglement length with both ends fixed in space. Our results for PE are just the opposite. Graf et al. argued that the strong residual orientation in polybutadiene could be caused by significant intermolecular orientation correlations. If this is correct, these correlations are apparently absent in polyethylene.

Kimmich and co-workers have used proton NMR to characterize the residual order of polyethylene remaining after segmental motion.[34] These results cannot be directly compared to those presented here because of the different observables (^{1}H vs ^{13}C) and the fact that the models used to fit the data use different regimes, rendering a close comparison difficult.

E. T_1 and NOE Values as a Function of Molecular Weight. Figure 1 shows that T_1 and NOE values from two samples with more than a factor of 2 difference in molecular weight (M) are the same within experimental error. Combined with our previous studies of unentangled PE, we conclude that T_1 and NOE varies with M for PE until some M between 2.1K and 16K. Further increases in M do not change T_1 and NOE values. This prediction is consistent with both models I and II. The precise M where this transition occurs depends on the temperature and the NMR Larmor frequency. Our conclusion is consistent with previous NMR studies on PE melts, suggesting 5300 g/mol as the molecular weight where T_1 and NOE are no longer a function of M.[32]

F. Nonexponential $T_{1\rho}$ Magnetization Decay. Figure 6 shows that the magnetization decay for the $T_{1\rho}$ experiment is nonexponential for PE16K. In contrast, an exponential magnetization decay is observed for the T_1 experiment for the same sample (shown as the inset in Figure 6). As shown in eq 5, the major difference between T_1 and $T_{1\rho}$ is that $T_{1\rho}$ has an additional low-frequency component. This low-frequency component is very sensitive to slow dynamics. Therefore, our results indicate that the fast segmental dynamics probed by T_1 are homogeneous over all chain positions while the slow global dynamics depend on position along the chain backbone. A reasonable explanation is that the center of the chain, which is heavily entangled, has much slower global dynamics than the end of the chain. Nonexponential magnetization decays were not observed in our earlier studies of unentangled PE (solid symbols in Figure 6), indicating that the global dynamics in an unentangled system are much more homogeneous. Thus, the combined results show that entanglements are very effective in slowing down the global dynamics for the center portion of a deeply entangled chain. Klein et al. have argued that excluding chain ends, of the order of one entanglement length, global dynamics are uniform along the chain.[35] We consider this to be unlikely although our present data would not exclude this possibility.

It has been observed as early as 1961 that high molar mass polymers exhibit nonexponential ^{1}H transverse magnetization decay.[36] The nonexponential $T_{1\rho}$ decay shown in Figure 6 provides another example of the complexity of polymer melt dynamics. ^{13}C experiments are easier to interpret than ^{1}H transverse magnetization decay experiments. The former is influenced by intramolecular motions since it monitors the reorientation of a bond connecting a ^{13}C nuclei and ^{1}H. The ^{1}H magnetization decay probes both reorientation of one chain and motion of neighboring chains relative to each other. Our modest molecular weight of 16K also ensures that semiclassical relaxation theory[37] is valid ($\tau_c \ll T_1$, T_2). Thus, the nonexponential magnetization decay ($T_{1\rho}$) observed in this study is not the result of experimental complications.

G. Characterizing Global Motions Using $T_{1\rho}$. Since $T_{1\rho}$ is sensitive to the global motions of polymer melts, it potentially serves as an effective probe of entanglements. The solid line in Figure 2 is the prediction of model II for PE16K. Although it has correct temperature dependence, the prediction is about 30% faster than the experimental data.

There are two possible reasons for the poor agreement. One possibility is that disentanglement dynamics in region III of model II are too slow. Several theories including constraint-release indicate disentanglement dynamics should be faster than predicted by the reptation model used in model II. The second possible cause is that our $T_{1\rho}$ calculation does not account for different dynamics as a function of position along the chain backbone. It may turn out if we model $T_{1\rho}$ on different chain positions individually and then calculate out the superimposed magnetization decay curve, the agreement will be better. However, even if we follow this suggestion and the agreement turns out to be favorable, the conclusion will be heavily model dependent.

The dashed line in Figure 2 is the prediction from model II for PE31K. The predicted $T_{1\rho}$ values are quite sensitive to molecular weight. Since $T_{1\rho}$, T_2, and field cycling measurements provide information about dynamics rather than structure, these methods may be useful for characterizing samples with very similar molecular weights but different viscoelastic behavior (perhaps because of branching).

V. Conclusion

^{13}C T_1, NOE, and $T_{1\rho}$ at 5 and 75 MHz ^{13}C Larmor frequencies were measured for two entangled PE melts. T_1 and NOE data are not influenced by molecular

weight above 15 700 g/mol. On the basis of our previous understanding of the segmental and global dynamics of unentangled PE melts, we constructed models that incorporate entanglement effects. From the comparison between predictions of the two models and the experimental data, we conclude that entanglement not only stretches the longest relaxation times of the chain but also has the effect of restricting the end points of an entanglement on the time scale of τ_e. The magnetization decay curve for the $T_{1\rho}$ experiment is nonexponential, indicating that the slow dynamics probed by the $T_{1\rho}$ experiment depends strongly on the position of the C−H vector along the chain.

This study provides a connection between two deeply related but historically independent NMR methods to study polymer dynamics: spin−lattice relaxation measurements for the segmental dynamics and transverse relaxation measurements for the global dynamics. Although our experiments are not optimal for study of either of the two dynamical regions, our work provides a broader perspective on each approach.

Acknowledgment. This research was supported by the National Science Foundation through the Division of Material Research, Polymer Program (DMR-0099849). We thank Prof. Tom Farrar, Marv Kontney, and Tom Ferris for help with the NMR measurements and Dr. Alessandro Faldi for providing one of the polyethylene samples.

Appendix

The following procedure was used to calculate the spectral density function for model II (described in the text) for chains with $M = 15\,700$ g/mol. The entanglement molecular weight M_e and the residual orientation left by Rouse motions between entanglement points A_{ent} are the two fitting parameters.

Following eq 6, $G_{seg}(t)$ is constructed as a single-exponential function with $\tau_{seg} = 7.5$ ps at 400 K and $E_{a,seg} = 4.0$ kcal/mol. A_{seg} is given in Table 1. The temperature dependence for the global motions $E_{a,nm}$ is taken to be the flow activation energy of 6.4 kcal/mol. $G_{nm}(t)$ is constructed from three functions which are all scaled by the relaxation time of a Rouse segment with 44 carbons τ_{44}. We get τ_{44} by multiplying τ_{44}/τ_{seg} from our study of unentangled PE[15] with τ_{seg} in this study. To simplify notation, we introduce the disentanglement time τ_d. A Rouse segment of 44 carbons is mode 25 for our chains. Thus, $\tau_d = (25/(M/M_e))^2(M/M_e)^{3.4}\tau_{44}$.

The dipolar interactions according to the reptation model have been described in detail by Callaghan and Samulski.[4] The global dynamics can be subdivided into three motional regions: free Rouse motion, Rouse motion constrained to the tube, and curvilinear diffusion in the tube. The first part of $G_{nm}(t)$, $G_{nm,Rouse}(t)$ (the free Rouse motion), is constructed following the procedure described in our previous study of unentangled polyethylene.[15] Since there are M/M_e entanglements in the PE chain, we stretch the relaxation time for the longest M/M_e modes by an extra factor of $M^{1.4}$ in excess of the Rouse scaling of M^2. $G_{nm,Rouse}(t)$ is restricted by entanglement points to relax to a residual orientation A_{ent}.

The second and third parts of $G_{nm}(t)$ are constructed heuristically from the behavior of the mean-square displacement (MSD) for a reptating chain. In the Rouse regime, it is well established that the MSD goes as $t^{1/2}$, while $G(t)$ goes as t^{-1}. For the second and third parts of $G_{nm}(t)$, we assume that $G(t)$ also goes as MSD^{-2}. The second part $G_{Rt}(t)$ corresponds to the Rouse motion constrained to a tube: $G_{Rt}(t) = (t/\tau_e)^{-0.5}$ for $\tau_e < t < \tau_R$. The third part $G_{cd}(t)$ corresponds to the curvilinear diffusion in the tube region is of the form

$$G_{cd}(t) = \left(\frac{t}{\tau_e}\right)^{-0.5}\left(\frac{t}{\tau_R}\right)^{-0.5}\left[\sum_{p\ \mathrm{odd}} \frac{8}{p^2\pi^2}\exp\left(\frac{-p^2 t}{\tau_d}\right)\right]^2 \quad \text{(A1)}$$

for $t > \tau_R$. τ_e and τ_R are related to the disentanglement time τ_d as $\tau_e = \tau_d/(M/M_e)^{3.4}$ and $\tau_R = \tau_d/(M/M_e)^{1.4}$. $G_{Rt}(t)$ and $G_{cd}(t)$ are normalized to create a continuous function:

$$G_{nm}(t) = (1 - A_{ent})G_{nm,Rouse}(t) + A_{ent} \quad \text{for } t < \tau_e$$

$$G_{nm}(t) = ((1 - A_{ent})G_{nm,Rouse}(\tau_e) + A_{ent})G_{Rt}(t) \quad \text{for } \tau_e < t < \tau_R$$

$$G_{nm}(t) = ((1 - A_{ent})G_{nm,Rouse}(\tau_e) + A_{ent})G_{cd}(t) \quad \text{for } t > \tau_R \quad \text{(A2)}$$

The resulting $G_{nm}(t)$ cannot be Fourier transformed analytically so an approximation was made with a sum of exponentials. Twelve exponentials are required to adequately describe the function. The time constant and the amplitude of these 12 exponentials are tabulated in Table 2. This approximation was then inserted into the expression for $G(t)$ (eq 6) which can be Fourier transformed analytically to yield the spectral density function. T_1, $T_{1\rho}$, and NOE can be calculated from the spectral density function following eqs 3−5.

Table 2. Parameters for the Multiexponential Approximation of $G_{nm}(t)$

amplitude	τ/τ_d	amplitude	τ/τ_d
0.0295	5.0×10^{-7}	0.009	2.0×10^{-3}
0.172	9.0×10^{-7}	0.004	1.0×10^{-2}
0.3	2.9×10^{-6}	0.003	0.025
0.3	8.5×10^{-6}	0.001	0.056
0.1	2.5×10^{-5}	0.0003	0.13
0.06	8.3×10^{-5}	0.0002	0.29
0.021	4.0×10^{-4}		

References and Notes

(1) Smith, G. D.; Paul, W.; Qiu, X. H.; Ediger, M. D. *Macromolecules* **1999**, *32*, 8857.
(2) Moe, N. E.; Qiu, X. H.; Ediger, M. D. *Macromolecules* **2000**, *33*, 2145.
(3) Bandis, A.; Wen W. Y.; Jones, E. B.; Kaskan, P.; Zhu, Y.; Jones, A. A.; Inglefield, P. T.; Bendler, J. T. *J. Polym. Sci., Polym. Phys. Ed.* **1994**, *32*, 1707.
(4) Callaghan, P. T.; Samulski, E. T. *Macromolecules* **1997**, *30*, 113.
(5) Brereton, M. G. *J. Chem. Phys.* **1991**, *94*, 2136.
(6) Graf, R.; Heuer, A.; Spiess, H. W. *Phys. Rev. Lett.* **1998**, *80*, 5738.
(7) Cohen-Addad, J. P.; Dupeyre, R. *Macromolecules* **1985**, *18*, 1101.
(8) Fatkullin, N.; Kimmich, R. *J. Chem. Phys.* **1994**, *101*, 822.
(9) English, A. D.; Inglefield, P. T.; Jones, A. A.; Zhu, Y. *Polymer* **1998**, *39*, 309.
(10) Cohen-Addad, J.-P. *J. Chem. Phys.* **1974**, *60*, 2440.
(11) deGennes, P.-G. *J. Chem. Phys.* **1971**, *55*, 572.
(12) Dejean de la Batie, R.; Lauprêtre, F.; Monnerie, L. *Macromolecules* **1988**, *21*, 2045.
(13) Smith, G. D.; Yoon, D. Y.; Zhu, W.; Ediger, M. D. *Macromolecules* **1994**, *27*, 5563.
(14) Cohen Addad, J. P. *Prog. NMR Spectrosc.* **1993**, *25*, 1.
(15) Qiu, X. H.; Ediger, M. D. *Macromolecules* **2000**, *33*, 490.
(16) Qiu, X. H.; Moe, N. E.; Ediger, M. D.; Fetters, L. J. *J. Phys. Chem.* **2000**, *113*, 2918.

(17) Qiu, X. H. Ph.D. Thesis, University of Wisconsin—Madison, 2000. Detailed information about probe construction is contained in this thesis.
(18) Glowinkowski, S.; Gisser, D. J.; Ediger, M. D. *Macromolecules* **1990**, *23*, 3520.
(19) Ohuchi, M.; Fujito, T.; Imanari, M. *J. Magn. Reson.* **1979**, *35*, 415.
(20) The averaged rate does not change more than 5% once we use at least three exponentials to fit the magnetization decay curve.
(21) Qiu, X. H.; Ediger, M. D. *J. Polym. Sci., Polym. Phys.* **2000**, *38*, 2634.
(22) Doddrell, D.; Glushko, V.; Allerhand, A. *J. Chem. Phys.* **1972**, *56*, 3683.
(23) Brereton, M. G. *Macromolecules* **1990**, *23*, 1119.
(24) Doi, M.; Edwards, F. *The Theory of Polymer Dynamics;* Clarendon: Oxford, 1986.
(25) Pearson, D. S.; Ver Strate, G.; von Meerwall, E.; Schilling, F. C. *Macromolecules* **1987**, *20*, 1133.
(26) Kimmich, R.; Weber, H. W. *J. Chem. Phys.* **1993**, *98*, 5847.
(27) Callaghan, P. T.; Samulski, E. T. *Macromolecules* **1998**, *31*, 3693.
(28) Pearson, D. S.; Fetters, L. J.; Graessley, W. W.; Ver Strate, G.; von Meerwall, E. *Macromolecules* **1994**, *27*, 711.
(29) Gell, C. B.; Graessley W. W.; Fetters L. J. *J. Polym. Sci., Polym. Phys.* **1997**, *35*, 1933.
(30) Richter, D.; Butera, R.; Fetters, L. J.; Huang, J. S.; Farago, B.; Ewen, B. *Macromolecules* **1992**, *25*, 6156.
(31) Pütz, M.; Kremer, K.; Grest, G. S. *Europhys. Lett.* **2000**, *49*, 735.
(32) Brereton, M. G.; Ward, I. M.; Boden, N.; Wright, P. *Macromolecules* **1991**, *24*, 2068.
(33) The factor "κ" in ref 35 accounts for this first averaging process.
(34) Huirua, T. W. M.; Wang, R.; Callaghan, P. T. *Macromolecules* **1990**, *23*, 1658.
(35) Klein, P. G.; Adams, C. H.; Brereton, M. G.; Ries, M. E.; Nicholson, T. M.; Hutchings, L. R.; Richards, R. W. *Macromolecules* **1998**, *31*, 8871.
(36) Powles, J. G.; Hartland, A.; Kail, J. A E. *J. Polym. Sci.* **1961**, *55*, 361.
(37) Redfield, A. G. *Adv. Magn. Reson.* **1965**, *1*, 1.

MA010597I